Complex electrical permittivity of the monolayer molybdenum disulfide (MoS_2) in near UV and visible

Bablu Mukherjee,[1] Frank Tseng,[2] Daniel Gunlycke,[2] Kiran Kumar Amara,[3] Goki Eda,[3] and Ergun Simsek[1,*]

[1]*The George Washington University, Washington, D.C. 20052, USA*
[2]*Naval Research Laboratory, Washington, D.C. 20375, USA*
[3]*National University of Singapore, Singapore*

[*]*simsek@gwu.edu*

Abstract: Temperature and Fermi energy dependent exciton eigen-energies of monolayer molybdenum disulfide (MoS_2) are calculated using an atomistic model. These exciton eigen-energies are used as the resonance frequencies of a hybrid Lorentz-Drude-Gaussian model, in which oscillation strengths and damping coefficients are obtained from the experimental results for the differential transmission and reflection spectra of monolayer MoS_2 coated quartz and silicon substrates, respectively. Numerical results compared to experimental results found in the literature reveal that the developed permittivity model can successfully represent the monolayer MoS_2 under different biasing conditions at different temperatures for the design and simulation of MoS_2 based opto-electronic devices.

© 2015 Optical Society of America

OCIS codes: (260.2110) Electromagnetic optics; (160.4760) Optical properties; (240.0310) Thin films.

References and links

1. R. F. Frindt and A. D. Yoffe, "Physical Properties of Layer Structures: Optical Properties and Photoconductivity of Thin Crystals of Molybdenum Disulphide," Proc. R. Soc. Lond. A **273**, 135269 (1963).
2. G. Eda, H. Yamaguchi, D. Voiry,T. Fujita, M. Chen, and M. Chhowallam, "Photoluminescence from Chemically Exfoliated MoS_2," Nano Lett. **11**, 5111 (2011).
3. T. Korn, S. Heydrich, M. Hirmer, J. Schmutzler, and C. Schuller, "Low-temperature photocarrier dynamics in monolayer MoS_2," Appl. Phys. Lett. **99**, 102109 (2011).
4. S.-L. Li, H. Miyazaki,H. Song, H. Kuramochi, S. Nakaharai, and K. Tsukagoshi, "Quantitative Raman Spectrum and Reliable Thickness Identification for Atomic Layers on Insulating Substrates," ACS Nano **6**, 7381 (2012).
5. C.-C. Shen, Y.-T. Hsu, L.-J. Li, and H.-L. Liu, "Charge Dynamics and Electronic Structures of Monolayer MoS_2 Films Grown by Chemical Vapor Deposition," Appl. Phys. Express **6**, 125801 (2013).
6. K. F. Mak, K. He, C. Lee, G. H. Lee, J. Hone, T. F. Heinz, and J. Shan, "Tightly bound trions in monolayer MoS_2," Nature Mat. **12**, 207 (2013).
7. A.K.M. Newaz, D. Prasai, J.I. Ziegler, D. Caudel, S. Robinson, R.F. Haglund Jr., K.I. Bolotin, "Electrical control of optical properties of monolayer MoS_2," Solid State Commun. **155**, 49 (2013).
8. J. -T. Liu, T.-B. Wang, X.-J. Li, and N.-H. Liu, "Enhanced absorption of monolayer MoS_2 with resonant back reflector," http://arxiv.org/abs/1403.0894.
9. W. Jin, P. C. Yeh, N. Zaki, D. Zhang, J. T. Sadowski, A. Al Mahboob, A. M. van der Zande, D. A. Chenet, J. I. Dadap, I. P. Herman, "Direct Measurement of the Thickness-Dependent Electronic Band Structure of MoS_2 Using Angle-Resolved Photoemission Spectroscopy," Phys. Rev. Lett. **111**, 106801 (2013).
10. J. S. Ross, S. Wu, H. Yu, N. J. Ghimire, A. M. Jones, G. Aivazian, J. Yan, D. G. Mandrus, D. Xiao, W. Yao, and X. Xu, "Electrical control of neutral and charged excitons in a monolayer semiconductor," Nature Comm. **4**, 1474 (2014).

#230586 - $15.00 USD Received 12 Dec 2014; revised 12 Jan 2015; accepted 15 Jan 2015; published 27 Jan 2015

11. Z. Li, S.-W. Chang, C.-C. Chen, and S. B. Cronin, "Enhanced photocurrent and photoluminescence spectra in MoS_2 under ionic liquid gating," Nano Research, **7**, 973–980 (2014).
12. C. Yim, M. O'Brien, N. McEvoy, S. Winters, I. Mirza, J. G. Lunney, and G. S. Duesberg, "Investigation of the optical properties of MoS2 thin films using spectroscopic ellipsometry," Appl. Phys. Lett. **104**, 103114 (2014).
13. H. Schmidt, S. Wang, L. Chu, M. Toh, R. Kumar, W. Zhao, A. H. Castro Neto, J. Martin, S. Adam, B. Ozyilmaz, and G. Eda, "Transport Properties of Monolayer MoS2 Grown by Chemical Vapor Deposition," Nano Letters **14** (4), 1909 (2014).
14. E. S. Kadantsev, P. Hawrylak, "Electronic Structure of a Single MoS_2 Monolayer," Solid State Commun. **152**, 909 (2012).
15. T. Cheiwchanchamnangij, W. R. Lambrecht, "Quasiparticle Band Structure Calculation of Monolayer, Bilayer, and Bulk MoS_2," Phys. Rev. B **85**, 205302 (2012).
16. A. Ramasubramaniam, "Large Excitonic Effects in Monolayers of Molybdenum and Tungsten Dichalcogenides," Phys. Rev. B **86**, 115409 (2012).
17. T. C. Berkelbach, M. S. Hybertsen, D. R. Reichman, "Theory of Neutral and Charged Excitons in Monolayer Transition Metal Dichalcogenides," Phys. Rev. B **88**, 045318 (2013).
18. D. Y. Qiu, F. H. da Jornada, and S. G. Louie, "Optical Spectrum of MoS_2: Many-Body Effects and Diversity of Exciton States", Phys. Rev. Lett. **111**, 216805 (2013).
19. F. Huser, T. Olsen, and K. S. Thygesen, "How dielectric screening in two-dimensional crystals affects the convergence of excited-state calculations: Monolayer MoS_2," Phys. Rev. B **88**, 245309 (2013).
20. E. J. G. Santos and E. Kaxiras, "Electrically Driven Tuning of the Dielectric Constant in MoS_2 Layers," ACS Nano **7**, 10741 (2013).
21. F. Tseng, E. Simsek, and D. Gunlycke, "Triangular Lattice Exciton Model," in preparation to be submitted, Jan. 2014.
22. S. Balendhran, J. Z. Ou, M. Bhaskaran, S. Sriram, S. Ippolito, Z. Vasic, E. Kats, S. Bhargava, S. Zhuiykov, Serge, and K. Kalantar-zadeh, "Atomically thin layers of MoS_2 via a two step thermal evaporation?exfoliation method," Nanoscale **2** 461 (2012).
23. Y. Shi, J.-K. Huang, L. Jin, Y.-T. Hsu, S. F. Yu, L.-J. Li, and H. Y. Yang, "Selective Decoration of Au Nanoparticles on Monolayer MoS2 Single Crystals," Sci. Rep. **3**, 1839 (2013).
24. J. R. Wait, "Transmission and reflection of electromagnetic waves in the presence of stratified media," J. Research NBS **61** (3), 205 (1958).
25. E.D. Palik, *Handbook of Optical Constants of Solids II* (Academic, 1991).

1. Introduction

Almost a half century ago, Frindt and Yoffe experimentally measured optical properties and photoconductivity of very thin crystals of molybdenum disulfide (MoS_2) as functions of crystal thickness and temperature [1]. According to their measurements, there are five very distinct absorption peaks occurring at the wavelengths of 666, 605, 448, 395, and 270 nm at the room temperature. When the temperature is lowered, these peaks experience both broadening and blue shifting. At very low temperatures, they also observed two small bands near the first peak (666 nm) and they assumed that the crystal tension was the main reason behind this effect. Unlike Frindt and Yoffe's work in which MoS_2 samples were prepared by mechanical cleavage, Eda *et al*. measured the structural and electronic properties of chemically exfoliated MoS_2 thin films and they concluded that above an annealing temperature of 300° C, chemically exfoliated MoS_2's semiconducting properties are largely restored [2].

In parallel to the growing attention on two-dimensional (2D) transition-metal dichalcogenides (TMDs), there are several experimental studies found in the recent literature presenting absorption and/or photoluminescence spectra in the visible and near ultra-violet (UV) parts of the electromagnetic spectrum as functions of layer number, temperature, and gate voltage [3–13]. Theoretical studies [14–21] confirm the high absorption capability of this material in the visible spectrum and its dependency on aforementioned factors.

In order to design and simulate opto-electronic devices built with MoS_2 or another similar 2D TMD, one needs to know its thickness (d) and complex electrical permittivity (ε_c). For the former, experimental and theoretical studies suggest $d = 0.65$ nm (about twice the in-plane lattice constant) for a monolayer MoS_2. For the latter, different studies [4, 5, 8] claim totally different results. Li *et al.* extract ε_c from the differential reflection spectrum using an effective

#230586 - $15.00 USD Received 12 Dec 2014; revised 12 Jan 2015; accepted 15 Jan 2015; published 27 Jan 2015
(C) 2015 OSA

reflection coefficient method [4], while Shen *et al.* use spectroscopic ellipsometry to calculate the refractive index [5]. Liu *et al.* first extract the imaginary part of ε_c from the absorption spectra, then calculate the real part using the Kramers-Kronig relation [8].

In this work, we follow a similar methodology. First, we measure the differential transmission (reflection) spectra through (from) an MoS_2 coated quartz (SiO_2/Si) substrate using broadband light sources both in visible and near UV. Second, we find the ε_c values as a function of wavelength, which yields almost the exact same differential transmission and reflection values for quartz and Si substrates, respectively, at each discrete wavelength sample of the measurement spectrum (300 nm $< \lambda <$ 1000 nm). Third, we develop an approximate expression for the ε_c as a function of wavelength. Since neither the Lorentz-Drude nor Gaussian model can describe the very dispersive nature of MoS_2 by itself, the proposed model is a combination of both, in other words it is a hybrid Lorentz-Drude-Gaussian model. As it is discussed below in detail, our method suggests much smaller values for the real part of ε_c compared to [4, 5].

In the last part, we discuss how to modify our model to capture the effects of temperature and gate voltage on ε_c using an atomistic model [21]. Basically, the subtraction of the Fermi energy corresponding to applied gate voltage from the valence band split successfully reflects both red and blue shifts occurring at the exciton eigen-energies [6]. A fitting equation proposed in [3] based on the standard semiconductor bandgap temperature dependency is utilized to make the model temperature dependent. Numerical results show a very good agreement with the experimental results found in literature obtained using MoS_2 on different substrates, applying a wide range of gate voltages, at different temperatures.

2. Sample preparation and characterization

The monolayer MoS_2 samples are grown by chemical vapor deposition technique on silicon substrates covered with 300 nm of silicon dioxide using [13]. It can be observed from the optical image (see the inset of Fig. 1(a)) that numerous large ($> 10\,\mu$m) crystallites of monolayer MoS_2 are formed. The triangular shape of most crystallites reflects the 3-fold symmetry of MoS_2 suggesting they are single-crystalline. Thus the optical image of the crystal formation signs the good crystalline quality. We have also performed Raman scanning and photoluminescence signal at different points of individual crystallites, which further reflect that they consist of a single crystal domain without any internal grain boundaries.

Figure 1(a) shows the Raman spectrum where the separation between two vibrating modes, E^1_{2g} and A_{1g}, is 20.4 cm^{-1}. Measurements taken at different spots indicate that this frequency difference is in the range of 20.4-20.7 cm^{-1}, confirming the film a homogeneous monolayer. The vibration mode of Mo-S bond (E^1_{2g}) along the base in-plane is observed at 385.4 cm^{-1} and vibration of sulfur along the out-of-plane (A_{1g}) is observed at 405.8 cm^{-1}, which further confirms the chemical purity of the sample where we do not observe any weak peaks in Raman signature corresponding to MoOx [22]. The FWHM of E^1_{2g} peak of the synthesized MoS_2 monolayer is 3.6 cm^{-1}, which suggests a good crystalline quality in the synthesized film.

Along with the electronic transport measurements, we can also get doping information of MoS_2 sample from Raman spectrum study [23]. It is reported that a detectable upshift of A_{1g} frequency and an increase of A_{1g}/E^1_{2g} peak intensity ratio suggest distinct *p*-doping material. In our experiment of Raman scanning, we measure the A_{1g}/E^1_{2g} peak intensity ratio of 1.54, which indicates that there could have native defects such as interstitials and vacancies present in the sample. Thus overall material can be summarized to be of high chemical purity but with native defects and good crystalline. However the photoluminescence spectrum of the sample further confirms and strongly supports the good sample quality. Intense and sharp band gap photoluminescence peak is observed from CVD grown monolayer MoS_2 sample, which also

#230586 - $15.00 USD Received 12 Dec 2014; revised 12 Jan 2015; accepted 15 Jan 2015; published 27 Jan 2015
(C) 2015 OSA

indicates the absence of substantial disorder in the as-grown sample.

For MoS_2 coated quartz substrates, we employ the same MoS_2 sample grown on SiO_2/Si substrate, where we transfer the sample from SiO_2/Si to quartz substrate in six steps as follows. First we spin-coat the MoS_2 covered Si/SiO_2 substrate with PMMA. Then thermal annealing of the PMMA coated substrate at 180° C for 5 minutes is performed. NaOH solution is used to etch SiO_2/Si substrate so that the film (PMMA coated MoS_2) floats. Later the film is cleaned in water (gently) and transferred on to quartz substrate and bake it once again to adhere to the quartz substrate. Then the sample is immersed in acetone for overnight duration to dissolve PMMA.

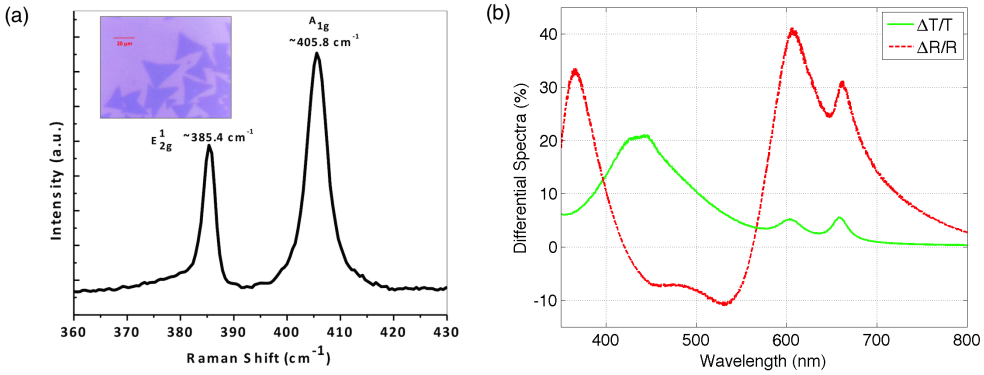

Fig. 1. (a) Raman spectrum of CVD monolayer MoS_2 on a SiO_2/Si substrate; inset is the optical image of as-synthesized films. (b) Measured differential transmittance through (green solid line) and reflectance from (red dashed line) MoS_2 coated SiO_2/Si and quartz substrates, respectively.

Raman and photoluminescence spectra are obtained using 532 nm excitation laser at excitation power of less than 150 μW to avoid sample damage. The measurements of differential reflectance from and transmittance through MoS_2 coated SiO_2/Si and quartz substrates, respectively, are performed using xenon and tungsten halogen lamps at room temperature and the results are plotted in Fig. 1(b). Note that differential transmission and reflection spectra are calculated using $\Delta T = (T_{\text{ref}} - T_{\text{sample}})/T_{\text{ref}}$ and $\Delta R = (R_{\text{ref}} - R_{\text{sample}})/R_{\text{ref}}$, respectively, where the subscripts "ref" and "sample" indicate measurements on bare and MoS_2 coated substrates.

3. Permittivity model

One can easily calculate the transmission through and reflection from a multilayered media using the transmission line analogy [24] if the thickness, permittivity, and permeability of each layer are known. Here, we treat the monolayer MoS_2 with an unknown permittivity, $\varepsilon_c(\omega)$, and known thickness, $d = 0.65$ nm. The wavelength dependent refractive indices of quartz, SiO_2, and Si are taken from [25]. The thickness of the SiO_2 layer is 300 nm. All the materials are assumed to be non-magnetic.

For the search algorithm, we create a mesh of complex $\varepsilon_c(\omega) = \varepsilon_r(\omega) + i\varepsilon_i(\omega)$ values, where the real (ε_r) and imaginary (ε_i) parts are linearly sampled along wide range of values. Then we adaptively calculate a specific ε_c value for each wavelength value available in our experimental results satisfying $\sqrt{(\Delta T_{\text{exp}} - \Delta T_{\text{num}})^2 + (\Delta R_{\text{exp}} - \Delta R_{\text{num}})^2} < 10^{-5}$, where the subscripts "exp" and "num" correspond to experimental and numerical results, respectively.

We plot the extracted complex electrical permittivity of MoS_2 in Fig. 2 and compare our results to the ones provided in [4, 5, 8]. Even though the imaginary parts look pretty similar

#230586 - $15.00 USD Received 12 Dec 2014; revised 12 Jan 2015; accepted 15 Jan 2015; published 27 Jan 2015
(C) 2015 OSA

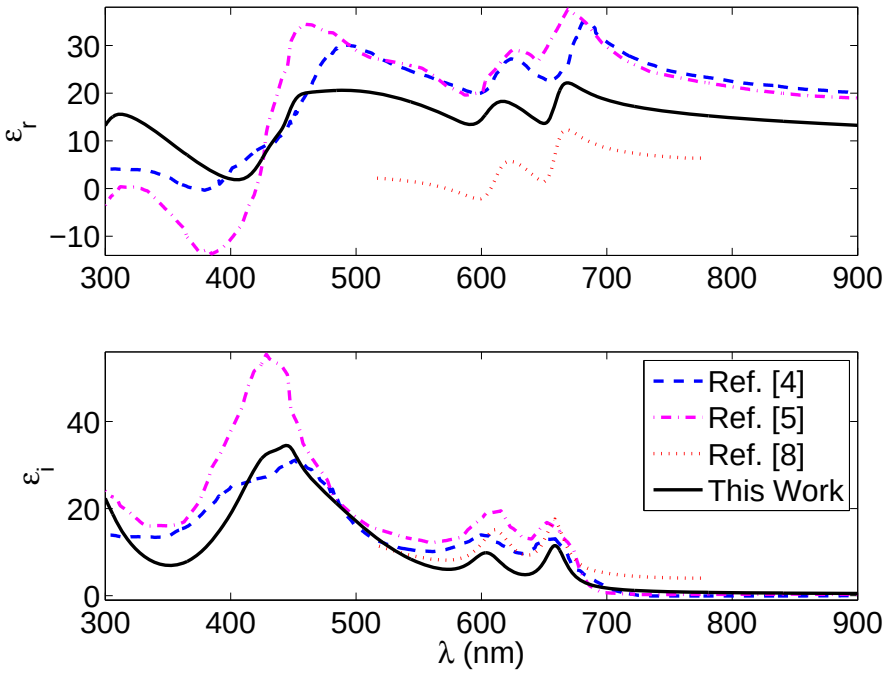

Fig. 2. Real (top) and imaginary (bottom) parts of the complex electrical permittivity of monolayer MoS_2. Black lines show the values extracted from our measurements, while blue dashed, magenta dashed-dotted, and red dotted lines are taken from references [4], [5], and [8], respectively.

to each other for $\lambda > 450$ nm, our results for the real part differ significantly from the others. Since the model proposed in [8] calculates the real part from the imaginary part, which uses only three oscillators (corresponding to the peaks occurring at 1.92, 2.08, and 2.88 eV), it is not surprising to see that their ε_r values are much smaller than our results (where we take all the 5 peaks into account) and the ones reported in [4] and [5]. On the other hand, Shen *et al.* claim a negative permittivity in the near UV part [5]. However, when we change the angle of incidence for 300 nm $\leq \lambda \leq$ 400 nm range, we did not observe any plasmonic effect in neither transmission nor reflection spectra. This is why ε_r should be positive in this region. Also, the permittivity model suggested in [4] does not have any signature of the absorption peak around 300 nm observed in our experiments and in [1, 2]. Last but not least, our result satisfies the Kramer-Kronig relations, i.e. the real part can be calculated from the imaginary part and vice versa. Under the light of these observations, we conduct multiple sets of numerical experiments to examine the accuracy of our model as follows.

In [6], Mak *et al.* experimentally measure the absorption of monolayer MoS_2 at different temperatures and gate voltages. Figure 3(a) compares their experimental results (at room temperature and a gate voltage of -70 V, which is very close to the undopped case) with our numerical results obtained with the multilayered medium code assuming same thickness (280 nm) for the SiO_2 layer as the substrate used in experiments and the permittivity values depicted in Fig. 2 for monolayer MoS_2. Figure 3(b) follows the same methodology for a suspended MoS_2 and compares our numerical results to the theoretical results provided in [18] obtained with a GW-Bethe-Salpeter equation solver. These two and all the other results (i.e. [8]), which are not provided here for the sake of brevity, show a very good agreement between the numerical

#230586 - $15.00 USD Received 12 Dec 2014; revised 12 Jan 2015; accepted 15 Jan 2015; published 27 Jan 2015
(C) 2015 OSA

results obtained with the permittivity values depicted in Fig. 2 and experimental results found in the literature for the absorption or differential reflection spectra of the monolayer MoS_2. As a result, we conclude that the complex permittivity of MoS_2 we extracted from our experiments can be safely used for the design and analysis of MoS_2 loaded structures operating at room temperature.

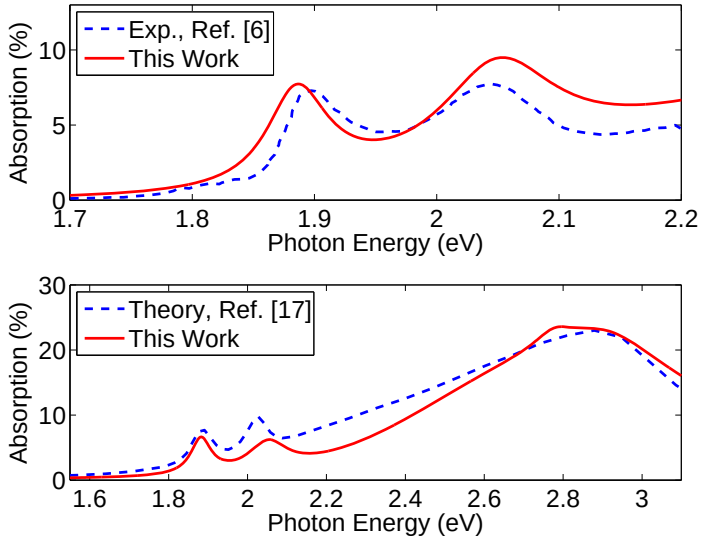

Fig. 3. Absorption spectrum of monolayer MoS_2 on top of a SiO_2/Si substrate (top) and residing in air (bottom). Blue dashed lines show experimental and theoretical results found in [6] and [18], respectively, whereas the red lines show our numerical results obtained with the ε_c values shown in Fig. 2.

3.1. A Hybrid Lorentz-Drude-Gaussian Model

For the numerical simulation of structures with dispersive materials, it is always advantageous to have a recipe to calculate each material's permittivity. In this direction, we first tried to approximate the ε_c using a Lorentz-Drude model with N of oscillators, where $3 < N < 10$. However, non of our trials were successful: the ones satisfying absorption peaks did not yield extremely low amount of absorption for $\lambda > 800$ nm or vice versa. This is why we decided to use a hybrid Lorentz-Drude-Gaussian (LDG) model, in which $\varepsilon_c = \varepsilon_c^{LD} + \varepsilon_c^{G}$, where the superscripts "LD" and "G" corresponds to Lorentz-Drude and Gaussian, respectively. The Lorentz-Drude part of the frequency dependent permittivity is given by

$$\varepsilon_c^{LD}(\omega) = \varepsilon_\infty + \sum_{j=0}^{5} \frac{a_j \omega_P^2}{\omega_j^2 - \omega^2 - i\omega b_j} \tag{1}$$

where ω_P is the plasma frequency, ε_∞ is DC permittivity, ω_j's, a_j's and b_j's are resonance frequency, oscillator strength, and damping coefficients, respectively, for the j^{th} oscillator. Basically, resonance frequencies are the ω values where we observe absorption peaks. In our experiments, they are found to be at 1.88 eV, 2.03 eV, 2.78 eV, and 2.91 eV, which agree well with the other experimental [1, 2, 6, 7] and theoretical [15, 16, 18, 21] studies. Herein, we adopt an atomistic model with the in-plane permittivity $\varepsilon_r^{\parallel} = 2.5$ and onsite $e-h$ interaction fitted to give resonance energies close to the observed peaks at 1.92, 2.08, 2.8, and 2.94 at $T = 0$ K.

#230586 - $15.00 USD Received 12 Dec 2014; revised 12 Jan 2015; accepted 15 Jan 2015; published 27 Jan 2015
(C) 2015 OSA

The other parameters used for the solution are lattice constant, $a_{lattice} = 0.316$ nm, valence band split, $E_{SO} = 0.152$ eV, and reduced mass $m = 0.32m_e$, where m_e is the mass of an electron. Considering the standard semiconductor bandgap temperature dependency, our experimental results obtained at room temperature are in good agreement with the theoretical results (roughly they are all 0.03-0.05 eV less than the theoretical results valid for $T = 0$ K). However the tail around 4 eV suggests another resonant frequency in the $\hbar\omega > 4$ eV region, which also appears in the experimental results [1, 2]. We assume this fifth resonant occurs at 4.34 eV.

For the Gaussian component, we first define the imaginary part as

$$\varepsilon_i^G(\omega) = \alpha \exp\left(-\frac{(\hbar\omega - \mu)^2}{2\sigma^2}\right), \tag{2}$$

which is a typical Gaussian distribution function with a mean of μ, variance of σ, and maximum value of α. Then we calculate the real part using Kramers-Kronig relation

$$\varepsilon_r^G(\omega) = -\frac{1}{\pi}\mathrm{PV}\int_{-\infty}^{\infty}\frac{\varepsilon_i^G(\omega')}{\omega' - \omega}d\omega'. \tag{3}$$

Using the experimentally measured plasma frequency of 28.3 meV, [5] in a non-linear least squares method, we find the optimum values for the unknown parameters in Eqs (1) and (2) as follows: $\varepsilon_\infty = 4.44$, $\alpha = 23.224$, $\mu = 2.7723$, $\sigma = 0.3089$, and a_j, b_j, ω_j values are listed in Table 1. In order to visualize the contributions of LD oscillators and Gaussian term, Fig. 4 shows 7 components (6 from LD and 1 from G) of the ε_i. Clearly, Gaussian component act like a carrier of the main behavior we observe in the absorption spectra and each LD oscillator corresponds to absorption peaks.

Table 1. Oscillation strength, damping coefficient, and resonance frequencies for the Lorentz-Drude oscillators used in (1). All coefficients are normalized with $\hbar$.

j	$a_j/\hbar$	$b_j/\hbar$	$\omega_j/\hbar$
0	2.0089×10^5	1.0853×10^{-2}	0
1	5.7534×10^4	5.9099×10^{-2}	1.88
2	8.1496×10^4	1.1302×10^{-1}	2.03
3	8.2293×10^4	1.1957×10^{-1}	2.78
4	3.3130×10^5	2.8322×10^{-1}	2.91
5	4.3906×10^6	7.8515×10^{-1}	4.31

3.2. Gate Voltage and Temperature Dependency

Experimental studies show that when a gate voltage is applied to a monolayer MoS_2 field-effect transistor, absorption spectrum changes [6–8, 11]. We observe three major effects: some of the peaks of spectrum gets smaller, wider, and shifted. Interestingly, when the applied voltage is increased, the first peak occurring at 1.92 eV experiences a blue-shift, while the second peak experiences a red shift. In terms of absorption, first two peaks are severely weaken with increased gate voltage, however, the rest does not change remarkably. With the help of the atomistic model, we can empirically make our hybrid LDG approximation gate voltage dependent as follows.

The atomistic model described in [21] uses a fixed value for the valence band split. When the gate voltage is applied to the transistor, the Fermi energy of MoS_2 changes. Fermi energy

#230586 - $15.00 USD Received 12 Dec 2014; revised 12 Jan 2015; accepted 15 Jan 2015; published 27 Jan 2015
(C) 2015 OSA

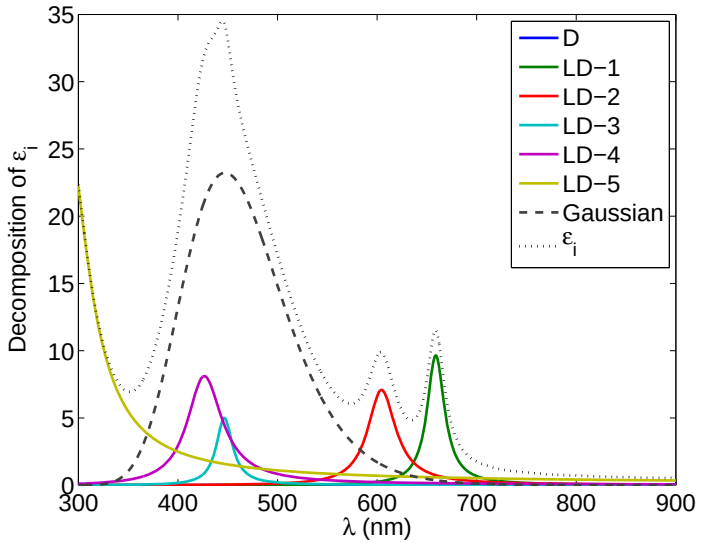

Fig. 4. Seven components of the ε_i, dottoed black line: Dashed gray line is the Gaussian term, all the other color lines are LD terms. Note that the first oscillator, $j = 0$ case that is also called Drude oscillator; has a very small imaginary part compared to others.

can be calculated analytically [6] using $E_F = \hbar^2 \pi C V_g / 0.7 m_e e^3$, where C is the back-gate capacitance, e is elementary charge, and V_g is gate voltage. Simply, by subtraction E_F from E_{SO}, the atomistic model becomes gate voltage dependent. Moreover, if we implement the temperature dependency model proposed in [3], the atomistic model can estimate the eigen-energies as functions of gate voltage and temperature. As listed in Table 2, all exciton energies decrease as the temperature is increased, whereas Fermi energy increase causes a blue shift on the first exciton eigen-energy and red shift on the second one. Note that these values perfectly agree with the experimental results found in the literature, i.e. [6].

Table 2. Exciton energies (E^A_{1s} and E^B_{1s}) calculated with the atomistic model at two different temperature values (10 K and 300 K) and Fermi energies (0 eV and 0.05 eV). All the exciton energies are presented in units of eV.

E_F	T (K)	E^A_{1s}	E^B_{1s}
0	10	1.92	2.08
0	300	1.88	2.05
0.05	10	1.93	2.07
0.05	300	1.896	2.038

In order to add peak weakening and broadening with the increased gate voltage, we simply multiply a_j's and divide b_j's with $\delta = e^{-12\pi(E_F - k_b T)^2}$, which is an empirically obtained term. Figure 5 shows comparisons of the absoption spectra obtained with the proposed approximation to experimental results [6] at two different temperatures assuming $C = 1.2 \times 10^{-8}$ F cm^{-2}. For the room temperature case, gate voltage is changed from -70 eV to 80 eV, corresponding to Fermi energy values changing from 9.5 meV to 48 meV. Numerical results show a good agreement with the experimental results. We also calculate the differential reflection spectra as

#230586 - $15.00 USD Received 12 Dec 2014; revised 12 Jan 2015; accepted 15 Jan 2015; published 27 Jan 2015
(C) 2015 OSA

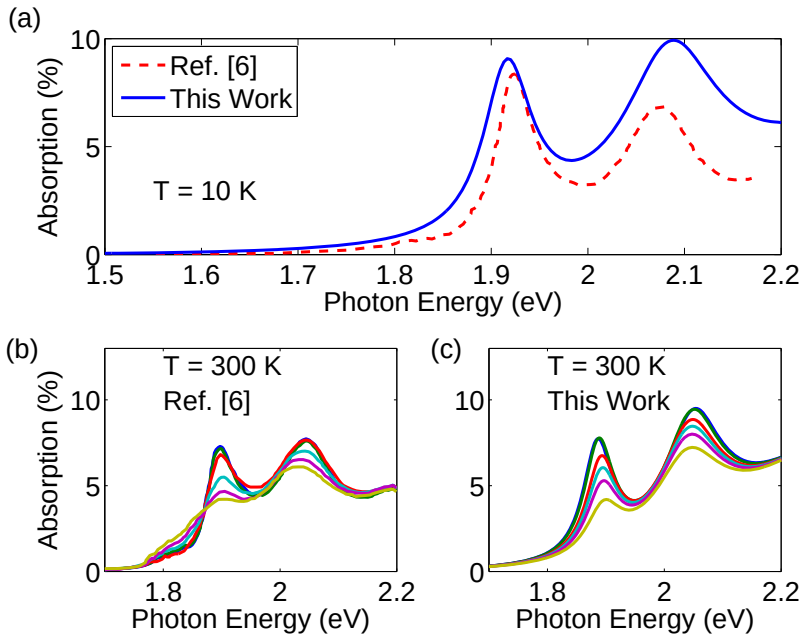

Fig. 5. Absorption spectrum of MoS_2 at $T = 10$ K (top) and $T = 300$ K. In (a), $V_g = -107$ V, corresponds to the undopped case, i.e. $E_F = 0$ eV [6]. In (b) and (c), gate voltage values are $V_g = (-70, -40, 10, 30, 50, 80)$ V. As V_g is increased, the absorption decreases (from blue to yellow lines).

a function of gate voltage and our numerical results agree well with the experimental results reported in [7].

Note that, Mak *et al.* have shown that *A* exciton peak evolves into two resonances [6], where one of these resonances diminishes rapidly with the applied gate voltage while the other one broadens gradually with almost constant strength. They conclude that the trion energy is the origin of the latter resonance and the splitting between the exciton and trion energies is a linear function of the Fermi energy. Since all the experiments we conducted were at room temperature, we could not clearly see the effect of trions in the absorption spectrum but one can easily add trions using an extra Lorentz-Drude oscillator to the approximation proposed above.

4. Conclusion

In conclusion, we extract the complex electrical permittivity of monolayer MoS_2 from differential transmission and reflection spectra experiments conducted on monolayer MoS_2 coated quartz and SiO_2 substrates. Then the extracted frequency dependent permittivity is approximated with a hybrid Lorentz-Drude-Gaussian model. Finally, this model is empirically modified to make it gate voltage and temperature dependent where the eigen-energies are calculated using an atomistic model. The accuracy of the model is verified through comparisons with the experimental results found in the literature for the wavelengths between 350 nm and 1 μm.

Acknowledgments

This work has been funded by the Office of Naval Research (ONR), directly and through the Naval Research Laboratory (NRL). E. S. and F. T. acknowledge support from NRL through the ONR Summer Faculty Program and the NRC Research Associateship Program, respectively.